RESEARCH ARTICLE

Thiazole Schiff Bases as Potential Breast Cancer Drugs through Design, Synthesis, and In Silico Analysis

Maher Afroj Khanam[1], Ranajit Kumar Sutradhar[1], Ashutosh Nath[2], Mamiya Chowdhury[3], Keya Rani Dutta[1], Sanjay Belowar[4]

1 Department of Chemistry, Chittagong University of Engineering and Technology, Bangladesh
2 Department of Chemistry, University of Massachusetts Boston, Boston, United States
3 Department of Chemistry, Dhaka University of Engineering and Technology, Bangladesh
4 Department of Natural Science, BGMEA University of Fashion and Technology, Dhaka, Bangladesh

Funding: No specific funding was received for this work.

Potential competing interests: No potential competing interests to declare.

Abstract

In this study, a series of thiazole-embedded Schiff base derivatives (TZ1-10) were investigated for their therapeutic potential against breast cancer, with TZ1-3 synthesized and TZ4-10 designed for comparative *in-silico* evaluation. Computational analyses, including Density Functional Theory (DFT) and molecular docking studies, revealed key electronic properties and binding affinities. The compounds exhibited HOMO-LUMO energy gaps indicating chemical stability, with TZ6 and TZ8 showing the most favorable values. ADMET profiling confirmed high bioavailability and low toxicity, with TZ6 and TZ8 showing ideal drug-likeness, positioning them as promising candidates for breast cancer therapeutics. Notably, TZ8 demonstrated a competitive binding affinity of -8.2 kcal/mol to the estrogen receptor (4FX3), comparable to FDA-approved drugs. These insights into stability, reactivity, and binding interactions provide a basis for future experimental validation, advancing the development of targeted cancer treatments with minimized adverse effects.

1. Introduction

Breast cancer remains one of the most common malignancies globally, impacting millions of women annually and substantially contributing to cancer mortality rates. Although targeted therapies have enhanced treatment outcomes, resistance to these therapies remains a major challenge[1][2]. Conventional treatments, such as chemotherapy, often cause severe side effects and may lead to tumor resistance, underscoring the need for novel, selective, and more effective anticancer agents[3][4]. In response to these issues, research has increasingly focused on developing small molecules with high specificity and minimal adverse effects.

Among various pharmacophores, Schiff bases and their derivatives have garnered significant interest in medicinal chemistry due to their structural versatility and potential bioactivity[5][6]. Schiff bases, often derived from thiosemicarbazones, exhibit remarkable anticancer, antimicrobial, and antioxidant properties, making them suitable

candidates for anticancer drug development[7][8][9]. Thiazole-based Schiff bases, in particular, have shown considerable promise, as the thiazole moiety enhances molecular stability and facilitates effective interactions with biological targets, including proteins involved in cell cycle regulation and apoptosis[10][11][12][13].

Recent advancements in computational methods, such as Density Functional Theory (DFT) and molecular docking, enable the *in-silico* evaluation of compounds' stability, reactivity, and binding affinity, facilitating the preclinical assessment of drug candidates[14][15][16][17]. By applying these computational tools, it is possible to identify and optimize novel compounds for enhanced bioactivity and pharmacokinetic profiles before conducting *in vitro* or *in vivo* studies[18][19].

In this study, we synthesized and computationally assessed a series of thiazole-embedded Schiff base derivatives (TZ1-10) for their potential as breast cancer therapeutics. Compounds TZ1-3 were synthesized, and the entire series (TZ1-10) underwent *in-silico* analyses to evaluate their binding affinity to estrogen receptors, an important target in hormone-dependent breast cancer. Furthermore, we examined the compounds' pharmacokinetic properties to determine their drug-likeness, bioavailability, and toxicity profiles. This research aims to identify promising lead compounds with the potential to serve as effective, safe, and accessible treatments for breast cancer, contributing to the development of targeted therapies with fewer side effects.

2. Materials and Methods

2.1. Materials

All starting materials and solvents used in the synthesis were procured from Sigma Aldrich and used without additional purification. Melting points of synthesized compounds were determined using an Electrothermal apparatus. Infrared spectra (IR) were measured using a SHIMADZU FTIR spectrophotometer (Model FTIR-IR Affinity-1) at Wazed Miah Scientific Research Centre, Jahangirnagar University, Savar, Dhaka, to confirm the presence of functional groups like NH, C=N, and C=S. Nuclear Magnetic Resonance (NMR) spectra, including ^{1}H and ^{13}C, were recorded using a BRUKER AVANCE III HD (400 MHz) spectrometer, with chemical shifts referenced in δ units to the residual protons in deuterated solvents. The spectral analyses for both IR and NMR were conducted at the Wazed Miah Science Research Centre, Jahangirnagar University, Bangladesh. These analyses facilitated the structural elucidation of the synthesized thiazole-embedded Schiff base derivatives.

2.2. Methods

2.2.1. *General Procedure for the Preparation of Thiosemicarbazone Derivatives (4-6)*

The synthesis of substituted thiosemicarbazone derivatives was conducted according to the method described by Al-Amiery[20]. The reaction took place in an acidic medium, combining 0.01 mol of 4-substituted benzaldehyde (1) and 0.01 mol of thiosemicarbazide (2) in 20 mL of ethanol. This mixture was refluxed at 60 °C for 3 hours. After cooling to room

temperature, the resulting-colored precipitate was filtered, washed with sodium bicarbonate solution, and recrystallized from 70% ethanol.

2.2.2. *Synthesis of Thiazole-Embedded Schiff Base Derivatives (TZ1-TZ3)*

A mixture of 0.013 mol of 3-chloroacetic acetone (3) and 0.015 mol of thiosemicarbazone derivatives (4-6) was dissolved in acetone and reflux 6 h. After completing reaction crude mixrue cooled in an ice bath. The cooled mixture was then added to ice-cold water to induce precipitation. The precipitate was filtered and recrystallized from ethanol, with compounds TZ1-TZ3 subsequently purified via column chromatography. Reaction shown in *Scheme 1*. All the reactions proceeded smoothly with diverse substituted thiosemicarbazone, and products were obtained in moderate yields. The structures of the synthesized compounds were elucidated by ^{1}H NMR, ^{13}C NMR, DEPT, HMBC spectroscopic method.

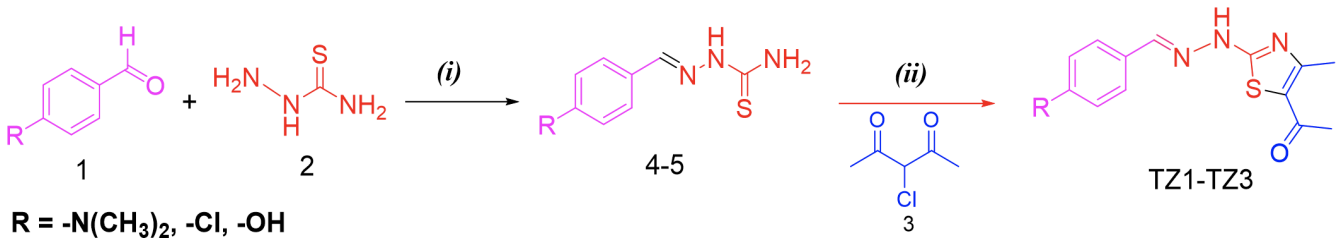

Scheme 1. Synthesis of thiosemicarbazone scaffold and thiazole-embedded Schiff base derivatives. The reaction conditions are as follows: (i) Catalytic amount of HCl in EtOH, reflux for 3 h at 60-70^{o}C, (ii) 3-chloroacetyl acetone in acetone, reflux for 6 h.

Physical properties of 2-(4-(dimethylamino) benzylidene) hydrazine-1-carbothioamide, 4:Orange colored powder, Yield 90%, m. p. 210~212 °C, IR (KBr, cm^{-1}, ***5***): 3406,3251(w, NH_2), 3051(C-H, Ar), 1593.99(C=N), 1184.29 (C=S), 815.85 (C-S-C). ^{1}HNMR (400 MHz, DMSO-d_6, δ ppm, ***5***): 7.59 (1H, d, J= 8.8 Hz, H-2′); 6.71 (1H, d, J= 8.4 Hz, H-3′);6.71 (1H, d, J= 8.4 Hz, H-5′) and 7.59 (1 H, d, J= 8.8 Hz, H-6′); 7.98 (1H, s, CH=N);3.36 (1H, s);11.04 (2H, s); 2.95 (2H, s). ^{13}C NMR (400 MHz, DMSO-d_6, δ ppm, ***5***): 121.8(C1'), 129.0(C2'), 112.1(C3'), 151.8(C4'), 112.1(C5'), 129.0(C6'), 143.8 (CH=N), 177.4(C=S),40.2N $(CH_3)_2$.

Physical properties of 2-(4-chlorobenzylidene) hydrazine-1-carbothioamide, 5:Brown coloured crystal, Yield 93%, m. p. 222~225 °C, IR (KBr, cm^{-1}, ***6***): 3468,3360(w, NH_2), 1587.47(C=N), 1234.44 (C=S), 877.46 (C-S-C). ^{1}HNMR (400 MHz, DMSO-d_6, δ ppm, ***6***): 7.59 (1H, d, J= 8.8 Hz, H-2′); 6.71 (1H, d, J= 8.4 Hz, H-3′);6.71 (1H, d, J= 8.4 Hz, H-5′) and 7.59 (1 H, d, J= 8.8 Hz, H-6′); 7.98 (1H, s, CH=N);3.36 (3H, s);2.95(2H, s). ^{13}C NMR (400 MHz, DMSO-d_6, δ ppm, ***6***): 125.5(C1'), 129.9(C2'), 116.0(C3'), 159.7(C4'), 116.0(C5'), 129.5 (C6'),143.2(CH=N), 177.8(C=S).

Physical properties of (E)-2-(4-hydroxybenzylidene) hydrazine-1-carbothioamide, 6:White powder, Yield 75%, m. p. 213 ~ 215 °C, IR (KBr, cm^{-1}, ***7***): 3560,3150.40(NH_2), 1612.40 (C=N), 1275.02 (C=S), 844.82 (C-S-C). ^{1}HNMR (400 MHz, DMSO-d_6, δ ppm, ***7***): 7.59 (1H, d, J= 8.8 Hz, H-2′); 6.71 (1H, d, J= 8.4 Hz, H-3′);6.71 (1H, d, J= 8.4 Hz, H-5′) and 7.59 (1 H, d, J= 8.8 Hz, H-6′); 7.98 (1H, s, CH=N);3.36 (3H, s);2.95(2H, s). ^{13}C NMR (400 MHz, DMSO-d_6, δ ppm, ***7***): 133.0(C1'), 129.4(C2'), 129.1(C3'), 134.7(C4'), 129.1(C5'), 129.4 (C6), 141.0(CH=N), 178.5(C=S).

Physical properties of 1-(2-(2-(4-(dimethylamino) benzylidene) hydrazineyl)-4-methylthiazol-5-yl) ethan-1-one, TZ1: Brown powder, Yield 55%, m.p.228~230 °C, IR (KBr, cm^{-1}, ***TZ1***): 3160 (NH), 3070 (w, C-H, Ar), 1604.77 (C=O), 1525.60 (C=N),1300.67, 1178.51 (C=S). ^{1}HNMR (400 MHz, DMSO-d_6, δ ppm, ***TZ1***: 7.50 (1H, d, J= 8.4 Hz, H-2′); 6.75 (1H, d, J= 8.4 Hz, H-3′);6.75 (1H, d, J= 8.4 Hz, H-5′); 7.50 (1H, d, J= 8.4 Hz, H-6′); 7.98 (1H, s, CH=N);3.38 (s);2.95(s). ^{13}C NMR (400 MHz, DMSO-d_6, δ ppm, ***TZ1***): 121.7(C1'), 129.0(C2'), 112.1(C3'), 151.9(C4'), 112.3(C5'), 129.0(C6'), 146.3(CH=N), 169.3(C=S), 111.5(C2"), 128.5(C4"), 189.0(C=O), 29.9($COCH_3$), 18.7(4"-$\underline{C}H_3$), 40.2N($\underline{C}H_3)_2$.

Physical properties of 1-(2-(2-(4-chlorobenzylidene) hydrazineyl)-4-methylthiazol-5-yl) ethan-1-one, TZ2: Light brown colored crystal, Yield 55%, m.p.190~192°C, IR (KBr, cm^{-1}, ***TZ2***): 3560, 3150 (NH), 3014.74, 2926 (w, C-H, Ar), 1612.40 (C=O), 1512.19 (C=N),1275.02 (C=S).^{1}HNMR (400 MHz, DMSO-d_6, δ ppm, ***TZ2***): 2.51(s, 3H, CO-CH_3), 2.41(s, 3H, H-4′), 7.55 (d,1H, H-2', J = 8.4 Hz), 6.86 (d, 1H, H-3′, J = 8.4 Hz), 6.86 (d,1H, H-5′, J = 8.4 Hz) and 7.55 (d,1H, H-5′, J = 8.4 Hz), 8.11 (s, 1H, CH=N). ^{13}C NMR (400 MHz, DMSO-d_6, δ ppm, ***TZ2***): 125.1(C1'), 129.2(C2'), 116.2(C3'), 160.1(C4'), 116.2(C5'), 129.2(C6'), 147.0($\underline{C}$H=N), 168.8($\underline{C}$=S), 122.0(C2"), 154.6(C4"), 189.3(C=O), 29.9(CO$\underline{C}H_3$), 17.9(4"-$\underline{C}H_3$).

Physical properties of 1-(2-(2-(4-hydroxybenzylidene) hydrazineyl)-4-methylthiazol-5-yl) ethan-1-one, TZ3: White colored powder, Yield 55%, m.p. 242~244°C, IR (KBr, cm^{-1}, ***TZ3***): 3414 (w, OH Ar),2738, 2645 (NH), 1622 (C=O), 1494 (C=N), 1240 (C=S). ^{1}HNMR (400 MHz, DMSO-d_6, δ ppm, ***TZ3***): 2.41(s, 3H, H-4′), 2.51(s, 3H, CO-CH_3), 5.38 (s,1H, NH), 7.72 (d,1H, H-2′, J = 8.0Hz), 7.51(d, 1H, H-3′, J = 8.4Hz), 7.51 (d,1H, H-5′, J = 8.4Hz), 7.72 (d,1H, H-6′, J = 8.0Hz), 8.16 (s,1H, HO-4′ and CH=N). ^{13}C NMR (DMSO-d_6, 400 MHz) δ: 133.0(C1'), 129.4(C2'), 129.1(C3'), 134.7(C4'), 129.1(C5'), 129.4 (C6), 141.0($\underline{C}$H=N), 178.5($\underline{C}$=S).

2.2.3. *Computational methods*

1. DFT Calculation

The structural properties of thiazole derivatives were modified and optimized using Gaussian 09[21] W Revision D.01. Visualization was carried out using Gauss View 6.0.16[21] software. Density Functional Theory (DFT) with the B3LYP functional and 6-311++G (d, p) basis set was applied to calculate spectral and physicochemical properties in the gas phase. Vibrational frequencies were confirmed to match minima on the potential energy surface, and molecular orbital characteristics were analyzed to assess chemical reactivity[19].

2. Thiazole Derivatives (TZ) Optimization, Protein Preparation, and Molecular Docking

Gauss View 6.0.16 was utilized to prepare the Gaussian input files (.gif) for Thiazole derivatives (TZ1-10). Each structure was optimized using Gaussian 09 and the B3LYP method. Protein structures were obtained from the RCSB Protein Data Bank (PDB). The specific proteins used were Homo sapiens *Spodoptera frugiperda* (PDB ID: 4FX3)[22] Homo sapiens Peptide from Nuclear receptor corepressor 2 (protein), Progesterone receptor (protein) (4OAR)[23] Homo sapiens Cell division protein kinase 6 (protein) (3NUP)[24] and Homo sapiens *Escherichia coli* (3ERT)[25] Prior to docking, water

molecules were removed, and original ligands were extracted. Ligands were docked against proteins using Autodock Vina[26] on the PyRx[27] workstation, with the grid box positioned around the macromolecule's active site. Visualization of receptor-ligand binding interactions was performed using Biovia Discovery Studio[28] 2024 Client.

3. Analysis of Drug Likeness of TZ1-10

Toxicity and pharmacokinetic properties were assessed using the updated AdmetSAR version 2.0[28] (http://lmmd.ecust.edu.cn/admetSAR2/). Drug-like properties of the compounds TZ (1-10) were analyzed using the Molinspiration online server[29] (https://www.molinspiration.com/cgi-bin/properties).

3. Result and Discussion

3.1. Chemistry

The structures of the synthesized compounds (TZ1-3) along with the designed compounds (TZ4-10) are shown in Figure 1. The spectral data of the synthesized thiazole-embedded Schiff base derivatives TZ1–TZ3 confirmed their structures through IR, ^{1}H NMR, and ^{13}C NMR spectroscopy. In the IR spectra, TZ1 showed absorptions at 3160 cm^{-1} for NH, 1604.77 cm^{-1} for C=O, and 1525.60 cm^{-1} for C=N[30]. For TZ2, peaks at 3560 and 3150 cm^{-1} corresponded to NH, with C=O and C=N absorptions at 1612.40 and 1512.19 cm^{-1}, respectively[31]. TZ3 exhibited a hydroxyl (-OH) group absorption at 3414 cm^{-1}, alongside C=O and C=N peaks at 1622 and 1494 cm^{-1}[31][32][33][34]. In ^{1}H NMR, characteristic singlet signals for CH=N were observed at around 7.98 ppm (TZ1 and TZ2) and 8.16 ppm (TZ3), confirming the Schiff base linkage[35]. ^{13}C NMR spectra further validated these structures, with characteristic C=N signals appearing between 141.0 and 147.0 ppm and C=O peaks ranging from 169.3 to 189.0 ppm[36]. This data collectively verifies the successful synthesis of the desired Schiff base compounds.

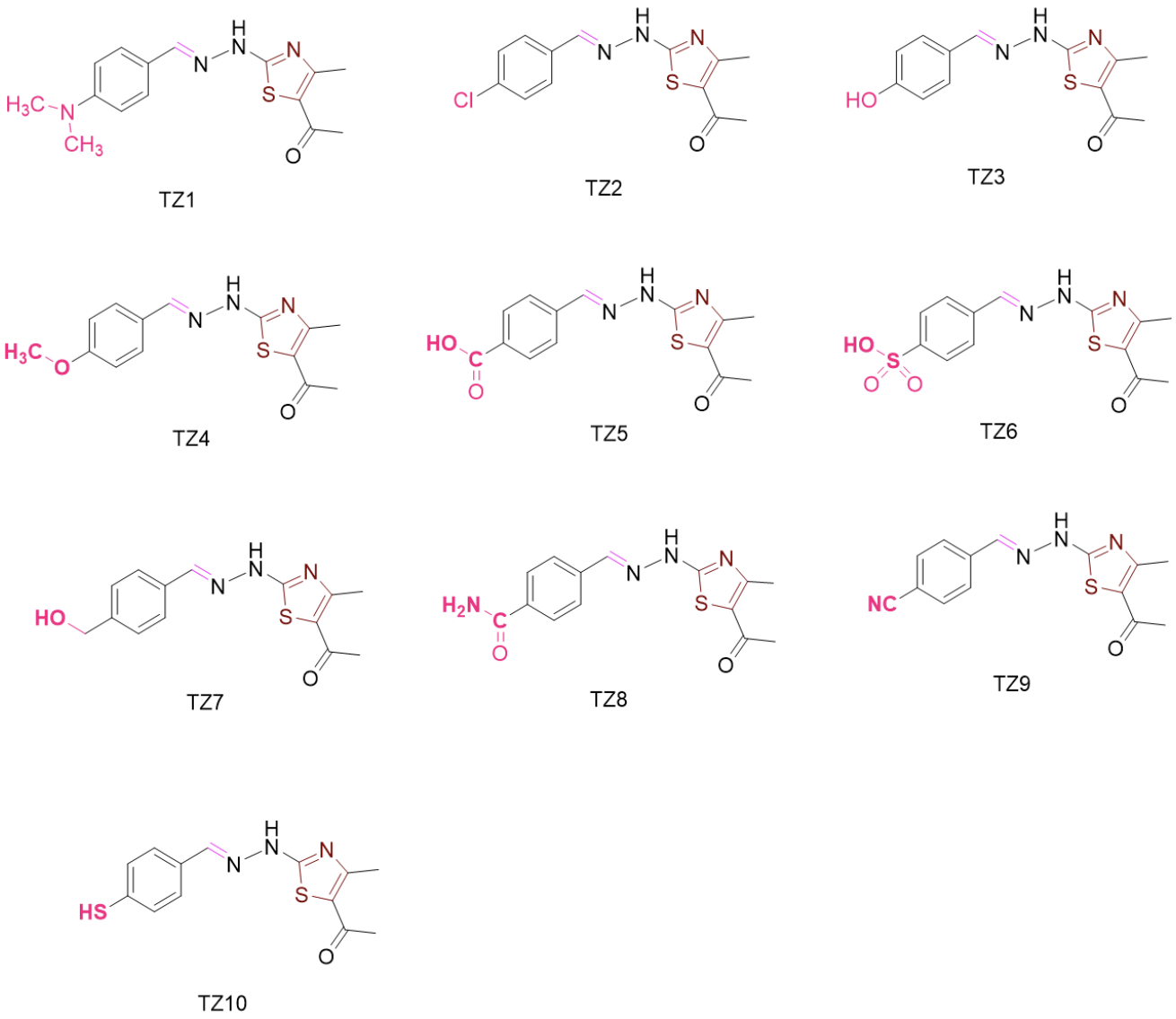

Figure 1. Designed new structures of thiazol derivatives

3.2. *In-silico* Study of Thiazole-Embedded Schiff Base Derivatives and Frontier Molecular Orbital Analysis

We designed ten Schiff base derivatives for further in-silico study, as illustrated in Figure 1. The optimized structures, shown in Figure S2, were calculated using Gaussian 09 W software, employing density functional theory (DFT) for optimization. Frontier molecular orbital (FMO) analysis was conducted to assess the Highest Occupied Molecular Orbital (HOMO) and the Lowest Unoccupied Molecular Orbital (LUMO), which play a crucial role in determining chemical reactivity. The HOMO reflects the ability of a molecule to donate electrons, while the LUMO indicates its capacity to accept electrons. The energy difference between these orbitals ($\Delta E = E_{LUMO} - E_{HOMO}$) is a key parameter for understanding the stability and reactivity of the compounds.

Table 1 presents the calculated values for E_{HOMO}, E_{LUMO}, and the energy gap (ΔE) for compounds TZ1-10. The HOMO energy values (E_{HOMO}) range from -0.17413 to -0.25362, indicating the highest occupied molecular orbitals. The LUMO energy values (E_{LUMO}) span from -0.05563 to -0.19278, representing the energy levels of the lowest unoccupied orbitals,

where more negative LUMO values suggest a greater ability to accept electrons. The HOMO-LUMO energy map is provided in Figure S1.

The HOMO-LUMO energy gap (ΔE) ranges from 0.02533 to 0.14029, with larger gaps indicating increased molecular stability. The hardness (η), representing the resistance to deformation of the electron cloud, shows negative values between 0.01267 and 0.07015. Softness (σ), which is inversely related to hardness, varies from 14.2572 to 78.9578, suggesting that compounds with higher softness may exhibit higher reactivity.

Electronegativity (μ) values range from -0.13966 to -0.2332, with more negative values indicating stronger electron-attracting tendencies. Chemical potential (χ) values, closely linked to electronegativity, vary from 0.11488 to 0.2232. Lastly, electronophilicity (ω) values, which are very low (0.111371 to 1.487589), suggest that these compounds have a limited tendency to accept electrons.

Table 1. Chemical reactivity of TZ1-10

TZs	E_{HOMO}	E_{LUMO}	ΔE	η	σ	μ	χ	ω
TZ1	-0.17413	-0.05563	0.1185	0.05925	16.8776	-0.11488	0.11488	0.111371
TZ2	-0.21524	-0.07496	0.14028	0.07014	14.2572	-0.1451	0.1451	0.150086
TZ3	-0.20127	-0.06098	0.14029	0.07015	14.2562	-0.13113	0.131125	0.122559
TZ4	-0.21783	-0.11970	0.09813	0.04907	20.3811	-0.16877	0.168765	0.290244
TZ5	-0.25362	-0.19278	0.06084	0.03042	32.8731	-0.2232	0.2232	0.81884
TZ6	-0.20678	-0.18145	0.02533	0.01267	78.9578	-0.19412	0.194115	1.487589
TZ7	-0.23287	-0.13715	0.09572	0.04786	20.8943	-0.18501	0.18501	0.357592
TZ8	-0.23464	-0.11653	0.11811	0.05906	16.9334	-0.17559	0.175585	0.261029
TZ9	-0.24895	-0.14713	0.10182	0.05091	19.6425	-0.19804	0.19804	0.385188
TZ10	-0.19957	-0.07974	0.11983	0.05992	16.6903	-0.13966	0.139655	0.16276

N.B.: global hardness (η), chemical potential (μ), softness (σ) electronegativity (χ), global electrophilicity index (ω).

3.3. Drug-likeness and Pharmacokinetic Characteristics

The molecular properties of TZ compounds, such as bioavailability and membrane permeability, are influenced by key factors like partition coefficient (logP), molecular weight (MW), and the number of hydrogen bond donors and acceptors, following Lipinski's "rule of five." As shown in Table 2, the molecular weight (MW) of these compounds ranges from 275.33 to 339.40 g/mol. Most of the TZ derivatives comply with Lipinski's rule, which applies to compounds with a molecular weight of less than 500 g/mol. The number of rotatable bonds ranges from four to six, where fewer rotatable bonds are often linked to improved bioavailability. The hydrogen bond properties show that most compounds have around six donors and one or two acceptors, both of which are crucial for solubility and receptor interactions. The Topological Polar Surface Area (TPSA) values range from 82.59 Å² to 145.34 Å², with lower TPSA (below 140 Å²) generally associated with better permeability and absorption, though TZ6 may have slightly reduced absorption. The consensus Log P values, indicating hydrophobicity, range from 1.71 to 3.30, with values between 1 and 3 typically showing optimal permeability and solubility.

Notably, TZ2 presents no Lipinski violations, shows low skin permeability (-5.29), has an excellent Log P (3.30), and a low molecular weight. TZ10 also stands out with no violations, an ideal Log P (2.99), and a low TPSA (121.39 Å²), while TZ9 exhibits good bioavailability due to its moderate Log P (2.54), acceptable molecular weight, and low TPSA.

Table 2. ADME properties of of TZ derivatives

TZ Derivatives	*MW (g/mol)*	*Num rotatable bonds*	*Num H bonds acceptors*	Num H bond donors	*TPSA (A2)*	*Consensus Log Po/w*	*Log Kp(skin permeation) cm/s*	*Lipinski rule*	*Violation*
TZ1	302.40	5	6	1	85.83	2.79	-5.70	Yes	0
TZ2	293.78	4	5	1	82.59	3.30	-5.29	Yes	0
TZ3	275.33	4	6	2	102.82	2.35	-5.87	Yes	0
TZ4	289.36	6	6	1	91.82	2.78	-5.73	Yes	0
TZ5	303.34	5	6	2	119.89	2.34	-6.13	Yes	0
TZ6	339.40	5	7	2	145.34	1.71	-6.90	Yes	0
TZ7	289.36	5	6	2	102.82	2.30	-6.34	Yes	0
TZ8	302.36	5	6	2	125.68	1.92	-6.58	Yes	0
TZ9	284.34	4	6	1	106.38	2.54	-5.88	Yes	0
TZ10	291.40	4	6	2	121.39	2.99	-5.61	Yes	0

Bioactivity score of TZ 1-10

The bioactivity scores of TZ compounds 1-10 were assessed. The drug-likeness of the lead compounds was evaluated using Molinspiration (https://www.molinspiration.com/cgi/properties), incorporating a range of factors, including GPCR modulators, ion channel modulators, kinase inhibitors, nuclear receptor ligands, protease inhibitors, and enzyme inhibitors (see Table 3). These combinations were analyzed to identify compounds suitable for further drug development. The bioactivity scores provide insights into the binding profiles of the compounds, which are useful in designing new drugs with improved selectivity and fewer side effects. Among the compounds, TZ6 displayed the fewest negative scores, suggesting higher overall bioactivity, particularly in its ability to bind GPCRs (-0.56) and inhibit enzymes (-0.28). TZ7 also demonstrated moderate activity, especially as a protease inhibitor (-1.08) and kinase inhibitor (-0.81).

Table 3. Bioactivity score of *TZ 1-10*

Drug	*GPCR ligand*	*Ion channel modulator*	*Kinase inhibitor*	*Nuclear receptor ligand*	*Protease inhibitor*	*Enzyme inhibitor*
TZ1	- 0.73	- 1.20	- 0.77	- 1.12	- 1.16	- 0.49
TZ2	- 0.90	- 1.29	- 1.00	- 1.38	- 1.39	- 0.58
TZ3	- 0.84	- 1.23	- 0.93	- 1.17	- 1.32	- 0.47
TZ4	- 0.86	- 1.31	- 0.93	- 1.25	- 1.29	- 0.56
TZ5	- 0.72	- 1.17	- 0.85	- 0.96	- 1.09	- 0.40
TZ6	- 0.56	- 1.02	- 0.88	- 1.34	- 0.81	- 0.28
TZ7	- 0.70	- 1.11	- 0.81	- 1.08	- 1.03	- 0.34
TZ8	- 0.72	- 1.25	- 0.67	- 1.27	- 1.03	- 0.43
TZ9	- 0.79	- 1.22	- 0.76	- 1.11	- 1.21	- 0.44
TZ10	- 0.96	- 1.47	- 1.14	- 1.53	- 1.25	- 0.49

3.4. Molecular Docking

3.4.1. *Protein selection*

Molecular docking is instrumental in drug discovery as it identifies potential therapeutic candidates, enhances the efficacy of existing medications, and elucidates the molecular basis of biological processes. This study selected proteins 4FX3, 4OAR, 3NUP, and 3ERT for their critical roles in hormone-dependent breast cancer and inflammation. Estrogen receptor alpha (4FX3) and aromatase (4OAR) are key in hormone signaling and cancer cell proliferation, making them vital for evaluating anti-cancer compounds. Nuclear Factor-kappa B (3NUP) regulates inflammation and cancer progression, while estrogen receptor beta (3ERT) is involved in apoptosis and hormone signaling. The thiazole-embedded Schiff base derivatives, particularly TZ6 and TZ8, demonstrated high binding affinities with these proteins, indicating potential as anti-cancer and anti-inflammatory agents. This targeted approach enhances the understanding of these compounds' therapeutic potential and guides further optimization for clinical applications. Table 5 shows that the TZ derivatives (TZ1-10) exhibit excellent docking performance, interacting with significant amino acids. Docking 55 complexes of four proteins with eleven TZ derivatives revealed specific protein targets related to the biological activity of the TZ drugs. TZ9 and TZ8 showed the highest affinities, indicating moderate interaction levels. Compounds like TZ2, TZ7, and TZ8 had strong interactions with the 3NUP receptor, highlighting its significance in the substance's mechanism of action. TZ9 and TZ8 also showed significant affinities, underscoring this receptor as crucial for the bioactivity of TZ drugs.

Table 4. Protein functions

PDB ID	Functions
4FX3	Phosphorylation of proteins involved in the G2, M transition by Cyclin A:Cdc2 complexes, cyclin A2-CDK1 complex, cell cycle G1/S phase transition, cellular response to cocaine, Transcription of E2F targets under negative control by p107 (RBL1) and p130 (RBL2) in complex with HDAC1
4OAR	glandular epithelial cell maturation, Loss of MECP2 binding ability to the NCoR/SMRT complex, negative regulation of androgen receptor signaling pathway, tertiary branching involved in mammary gland duct morphogenesis
3NUP	Multivesicular body, internal vesicle lumen, negative regulation of cardiocyte differentiation, positive regulation of protein kinase C activity, Shc-EGFR complex, epidermal growth factor receptor activity
3ERT	G protein-coupled estrogen receptor activity, regulation of epithelial cell apoptotic process, antral ovarian follicle growth, regulation of branching involved in prostate gland morphogenesis,

Table 5. Molecular Docking scores of selected TZ1-10 compounds with the four receptors.

Compound/Docking score (k/cal)	4FX3	4OAR	3NUP	3ERT
TZ1	-6.7	-7.3	-7.0	-6.6
TZ2	-7.8	-7.7	-7.6	-6.5
TZ3	-7.6	-7.6	-7.2	-6.8
TZ4	-7.4	-7.6	-6.6	-6.6
TZ5	-7.9	-7.4	-6.8	-7.6
TZ6	-8.0	-7.6	-6.8	-7.1
TZ7	-7.7	-7.6	-6.5	-7.1
TZ8	-8.2	-7.5	-7.0	-7.3
TZ9	-7.9	-7.8	-6.4	-7.4
TZ10	-7.2	-6.7	-6.3	-6.5

In Table 6, derivatives TZ8 and TZ6 demonstrated the highest binding affinities towards the 4FX3 receptor, with docking scores (S) of -8.2 and -8.0 kcal/mol, respectively. The derivative TZ8 formed three hydrogen bonds with LEU83 at distances of 1.95 Å, 2.25 Å, and 2.11 Å, and three hydrogen bonds with PHE82. Derivative TZ6 exhibited the formation of five hydrogen bonds involving LYS33, ASP86, LEU83, GLN85, with distances of 2.46 Å, 2.10 Å, 2.47 Å, 2.79 Å, and 2.83 Å, respectively. However, TZ5 and TZ9 displayed different interactions with 4FX3 despite having identical binding affinities. TZ5 established five hydrogen bonds with LEU83, LYS33, and GLN85, at distances of 2.35 Å, 2.67 Å, 2.16 Å, 2.73 Å, and 2.60 Å, respectively. TZ9 formed two hydrogen bonds with LEU83 and PHE82 at distances of 1.20 Å and 2.77 Å.

Table 6. Molecular Docking score of FDA approval drug

FDA approved drugs	4FX3	4OAR	3NUP	3ERT
Anastrozole	-8.1	-6.8	-8.2	-7.9
Doxorubicin	-8.5	-8.3	-8.4	-7.8
Gemcitabine	-7.6	-6.7	-6.6	-7.3
Tamoxifen	-5.7	-8.5	-6.2	-5.7

FDA-approved drugs generally exhibit stronger binding affinities, with Doxorubicin and Tamoxifen displaying the lowest energy values (-8.4 and -8.5 kcal/mol, respectively). Among the TZ compounds, TZ8 shows the strongest binding with the 4FX3 receptor (-8.2 kcal/mol), which is comparable to the binding strength of Doxorubicin. The binding affinities of FDA-approved medications range from -5.7 to -8.5 kcal/mol. Compared to these medications, the TZ compounds demonstrate slightly weaker binding strengths, ranging from -6.3 to -8.2 kcal/mol. FDA-approved medications generally exhibit greater and more consistent binding across receptors compared to the TZ1-10 compounds. This suggests that while FDA-approved medications may be more efficient, the TZ compounds—notably TZ8—still show competitive binding, particularly with 4FX3. These findings indicate the potential for further optimization of TZ compounds to enhance their binding affinities to levels comparable to or exceeding those of FDA-approved medications.

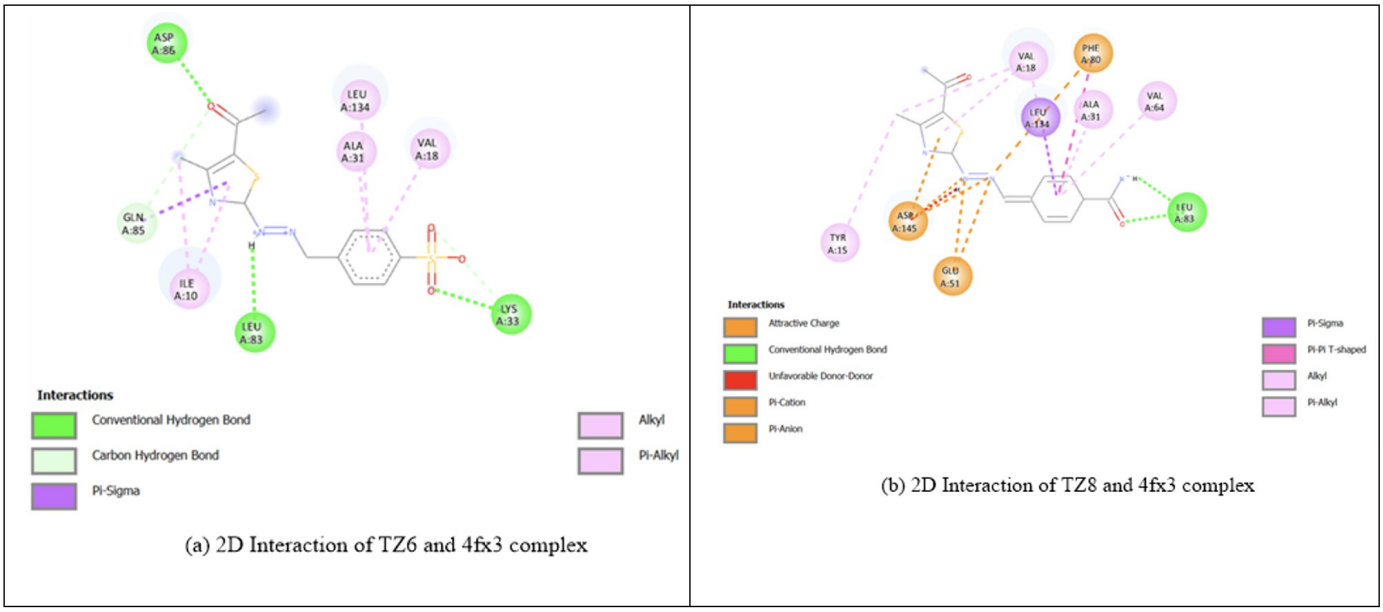

Figure 2. (a) 2D Interection of TZ6 + 4fx3 complex. (b) 2D Interection of TZ8 + 4fx3 complex.

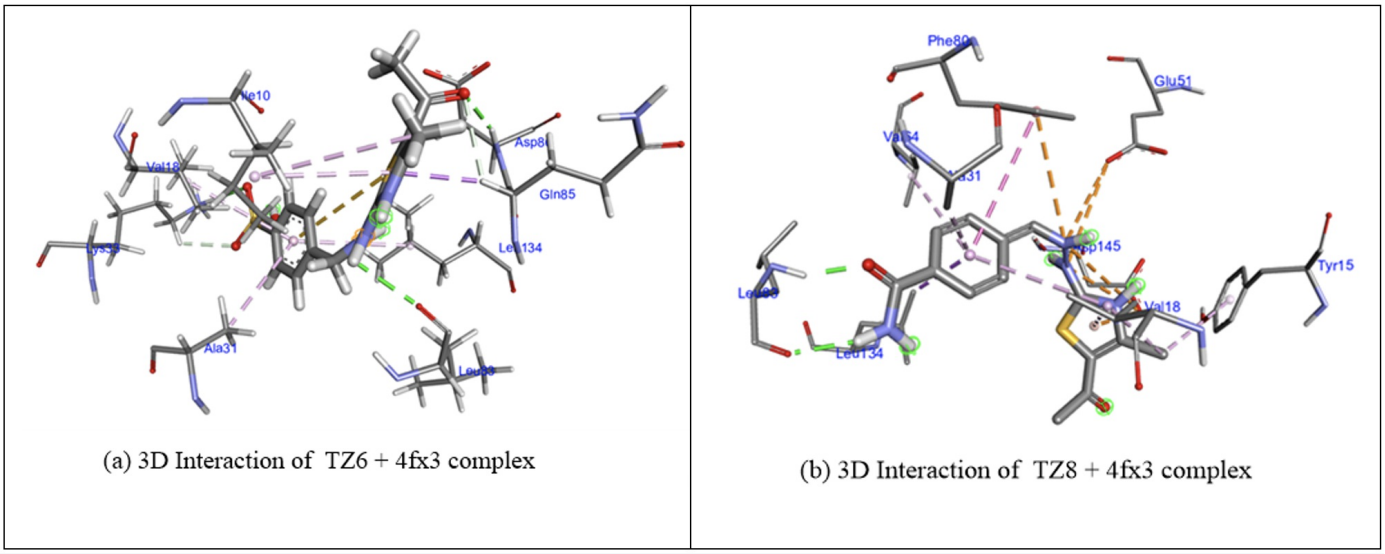

Figure 3. (a) 3D Interection of TZ6 + 4FX3 complex. (b) 3D Interection of TZ8 + 4FX3 complex.

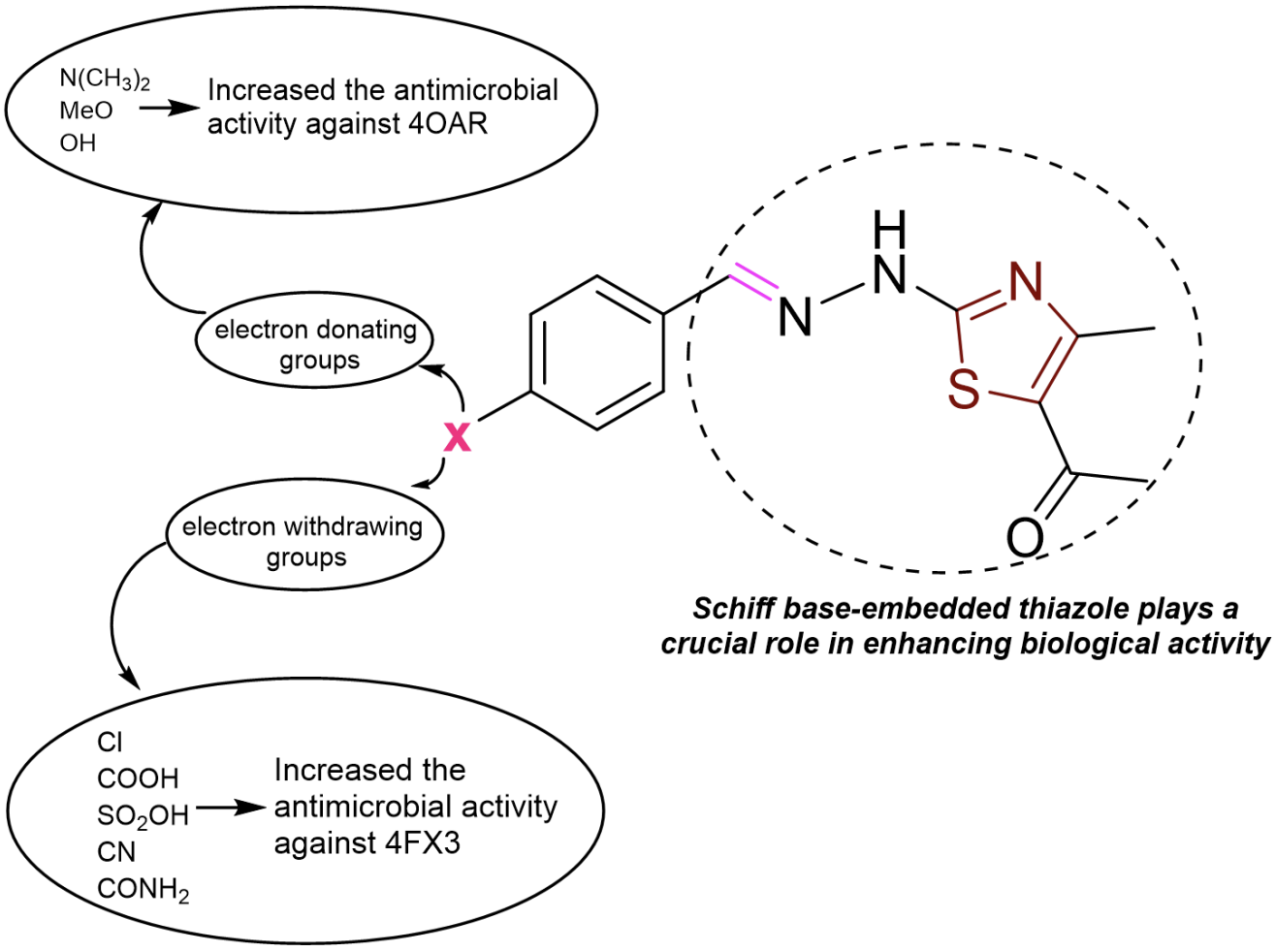

Figure 4. Structure activity relationship study of the TZ derivatives.

Figure 4 illustrates the crucial role of electron-donating and electron-withdrawing groups in modulating the antibacterial activity of a thiazole-based compound. The figure demonstrates the impact of substituents on the antibacterial properties

of the compound, highlighting the significance of these groups in controlling biological activity. At the core of the figure is a thiazole ring structure, renowned for its biological relevance in numerous medicinal compounds. The basic structure being studied consists of an aryl group and an acetyl group attached to the thiazole ring. The letter "X" marks a position on the aryl ring where various substituents can be introduced, significantly altering the compound's antibacterial action.

The figure 4 reveals that antimicrobial activity against the 4OAR strain is enhanced by the introduction of electron-donating groups such as dimethylamino ($N(CH_3)_2$), methoxy (MeO), and hydroxy (OH) at the X position. These groups increase the electron density of the ring, potentially improving the compound's efficacy by strengthening its interaction with microbial enzymes or cell membranes. Conversely, electron-withdrawing groups like cyano (CN), amide ($CONH_2$), sulfonic acid (SO_2OH), carboxylic acid (COOH), and chloride (Cl) enhance antibacterial activity against the 4FX3 strain. These groups decrease the electron density of the ring, which may heighten the molecule's binding affinity to microbial targets and boost its antibacterial activity.

Moreover, the figure clearly shows that modifying the substituents at the X position can fine-tune the antibacterial activity of the thiazole-based molecule. The distinct roles of electron-donating and electron-withdrawing groups in targeting different bacterial strains provide a strategic approach to developing more effective antimicrobial drugs.

4. Conclusion

In contrast to four FDA-approved breast cancer medicines, this study focuses on the synthesis and in-silico assessment of ten new thiazole-embedded Schiff base derivatives (TZ1–10). Notably, TZ6 and TZ8 demonstrated noteworthy docking scores above -6 kcal/mol, as well as excellent oral bioavailability and encouraging ADME characteristics. These substances showed low toxicity and no carcinogenic qualities, as well as substantial binding affinities, especially towards the 4FX3 protein. According to the knowledge gained from this study, TZ6 and TZ8 have a great deal of promise as anticancer drugs. In order to increase these compounds' binding affinities and boost their therapeutic efficacy, future research will concentrate on improving their molecular structure. Furthermore, to validate these computational predictions and evaluate the complete pharmacological potential of these derivatives, in-vitro and in-vivo investigations are required. These initiatives may eventually aid in the creation of fresh, more focused, and efficient therapies for breast cancer, providing a substitute for the current ones, which frequently have unfavorable side effects and resistance.

Statements and Declarations

Conflict of Interests

The authors declare no competing financial interest.

Acknowledgments

We are grateful to the Chittagong University of Engineering and Technology (CUET), Chattogram, Bangladesh for all kinds of experimental and financial supports.

References

1. ^*Hameed A, Al-Rashida M, Uroos M, Abid Ali S, Khan KM. Schiff bases in medicinal chemistry: a patent review (2010-2015). Expert opinion on therapeutic patents 2017; 27(1): 63-79.*
2. ^*Bharti S, Nath G, Tilak R, Singh S. Synthesis, anti-bacterial and anti-fungal activities of some novel Schiff bases containing 2, 4-disubstituted thiazole ring. European journal of medicinal chemistry 2010; 45(2): 651-660.*
3. ^*Docherty JH, Lister TM, Mcarthur G, Findlay MT, Domingo-Legarda P, Kenyon J, Choudhary S, Larrosa I. Transition-metal-catalyzed C–H bond activation for the formation of C–C bonds in complex molecules. Chemical Reviews 2023; 123(12): 7692-7760.*
4. ^*Mushtaq I, Ahmad M, Saleem M, Ahmed A. Pharmaceutical significance of Schiff bases: An overview. Future Journal of Pharmaceutical Sciences 2024; 10(1): 16.*
5. ^*Teran R, Guevara R, Mora J, Dobronski L, Barreiro-Costa O, Beske T, Pérez-Barrera J, Araya-Maturana R, Rojas-Silva P, Poveda A. Characterization of antimicrobial, antioxidant, and leishmanicidal activities of Schiff base derivatives of 4-aminoantipyrine. Molecules 2019; 24(15): 2696.*
6. ^*Çakmak R, Ay B, Çınar E, Başaran E, Akkoç S, Boğa M, Taş E. Synthesis, spectroscopic, thermal analysis and in vitro cytotoxicity, anticholinesterase and antioxidant activities of new Co (II), Ni (II), Cu (II), Zn (II), and Ru (III) complexes of pyrazolone-based Schiff base ligand. Journal of Molecular Structure 2023; 1292: 136225.*
7. ^*Kostova I, Saso L. Advances in research of Schiff-base metal complexes as potent antioxidants. Current medicinal chemistry 2013; 20(36): 4609-4632.*
8. ^*El-Lateef HMA, El-Dabea T, Khalaf MM, Abu-Dief AM. Recent overview of potent antioxidant activity of coordination compounds. Antioxidants 2023; 12(2): 213.*
9. ^*Pisanu F, Sykula A, Sciortino G, Maseras F, Lodyga-Chruscinska E, Garribba E. Experimental and Computational Studies on the Interaction of DNA with Hesperetin Schiff Base CuII Complexes. International journal of molecular sciences 2024; 25(10): 5283.*
10. ^*Oladipo SD, Luckay RC, Olofinsan KA, Obakachi VA, Zamisa SJ, Adeleke AA, Badeji AA, Ogundare SA, George BP. Antidiabetes and antioxidant potential of Schiff bases derived from 2-naphthaldehye and substituted aromatic amines: Synthesis, crystal structure, Hirshfeld surface analysis, computational, and invitro studies. Heliyon 2024; 10(1).*
11. ^*Arshad MF, Alam A, Alshammari AA, Alhazza MB, Alzimam IM, Alam MA, Mustafa G, Ansari MS, Alotaibi AM, Alotaibi AA. Thiazole: A versatile standalone moiety contributing to the development of various drugs and biologically active agents. Molecules 2022; 27(13): 3994.*
12. ^*Petrou A, Fesatidou M, Geronikaki A. Thiazole ring—A biologically active scaffold. Molecules 2021; 26(11): 3166.*
13. ^*Rani M, Nath A, Kumer A. In-silico investigations on the anticancer activity of selected 2-aryloxazoline derivatives against breast cancer. Journal of Biomolecular Structure and Dynamics 2023; 41(17): 8392-8401.*

14. ^Choi JE, Kim Z, Park CS, Park EH, Lee SB, Lee SK, Choi YJ, Han J, Jung KW, Kim HJ. Breast cancer statistics in Korea, 2019. Journal of Breast Cancer 2023; 26(3): 207.
15. ^Esteva FJ, Hubbard-Lucey VM, Tang J, Pusztai L. Immunotherapy and targeted therapy combinations in metastatic breast cancer. The lancet oncology 2019; 20(3): e175-e186.
16. ^Xia Y, Sun M, Huang H, Jin WL. Drug repurposing for cancer therapy. Signal Transduction and Targeted Therapy 2024; 9(1): 92.
17. ^Nath A, Kumer A, Zaben F, Khan MW. Investigating the binding affinity, molecular dynamics, and ADMET properties of 2, 3-dihydrobenzofuran derivatives as an inhibitor of fungi, bacteria, and virus protein. Beni-Suef University Journal of Basic and Applied Sciences 2021; 10(1): 36.
18. ^Sarkar M, Nath A, Kumer A, Mallik C, Akter F, Moniruzzaman M, Ali MA. Synthesis, molecular docking screening, ADMET and dynamics studies of synthesized 4-(4-methoxyphenyl)-8-methyl-3, 4, 5, 6, 7, 8-hexahydroquinazolin-2 (1H)-one and quinazolinone derivatives. Journal of Molecular Structure 2021; 1244: 130953.
19. a, bNath A, Kumer A, Khan MW. Synthesis, computational and molecular docking study of some 2, 3-dihydrobenzofuran and its derivatives. Journal of Molecular Structure 2021; 1224: 129225.
20. ^Al-Amiery A, Isahak WNRW, Al-Azzawi WK. Multi-method evaluation of a 2-(1, 3, 4-thiadiazole-2-yl) pyrrolidine corrosion inhibitor for mild steel in HCl: combining gravimetric, electrochemical, and DFT approaches. Scientific Reports 2023; 13(1): 9770.
21. a, bCaricato M, Frisch MJ, Hiscocks J, Frisch MJ. Gaussian 09: IOps Reference; Gaussian Wallingford, CT, USA, 2009.
22. ^Li C, Xie Y, Hu S, Yu H, Xu Y, Shen H, Yuan Y, Gu L, Pu B. Identification of formononetin as the active compound of CR-SR in hepatocellular carcinoma treatment: An integrated approach combining network pharmacology and weighted gene co-expression networks. Chemical Biology & Drug Design 2024; 103(1): e14363.
23. ^Kitete Mulongo E, Kilembe Thambwe J, Matondo A, Ngbolua K-T-N, Tshilanda D, Mungu Yvette N-U, Tshibangu D, Tshimankinda Mpiana P. The Potential of Compounds Derived from Jatropha Curcas Against Pr and Herα in Breast Cancer Treatment: Molecular Docking and Molecular Dynamics Simulation Studies.
24. ^Jiang C, Ye Y, Kang W, Yang J, He Z, Cao Q, Lian C, Xing Y, Yang Q, Zhao J. Elucidating Binding Selectivity in Cyclin-Dependent Kinases (CDKs) 4, 6, and 9: Development of Highly Potent and Selective CDK4/9 Inhibitors. 2024.
25. ^Somturk-Yilmaz B, Turkmenoglu B, Akkoc S. Synthesis, Characterization, Cytotoxic Activity Studies of N1-phenylbenzene-1, 2-diamine@ CuhNFs and 1, 2-phenylenediamine@ CuhNFs, and Molecular Docking Calculations of Their Ligands. Journal of Inorganic and Organometallic Polymers and Materials 2024; 1-13.
26. ^Trott O, Olson AJ. AutoDock Vina: improving the speed and accuracy of docking with a new scoring function, efficient optimization, and multithreading. Journal of computational chemistry 2010; 31(2): 455-461.
27. ^Dallakyan S, Olson AJ. Small-molecule library screening by docking with PyRx. Chemical biology: methods and protocols 2015; 243-250.
28. a, bJejurikar BL, Rohane SH. Drug designing in discovery studio. 2021.

29. ^*Suganya M, Jose Kavitha S, Raja Kannan V. Insilco Studies of Molecular Property and Bioactivity of Organic Crystalline Compounds using Molinspiration. International Research Journal of Engineering and Technology 2020.*

30. ^*Preethi V, Vijukumar V, AnilaRaj S, Vidya V. Synthesis, characterization, DFT studies and evaluation of the potential anti-tumour activity of nicotinic hydrazide based Schiff base using in vitro and molecular docking techniques. Heliyon 2024; 10(9).*

31. a, b*Belowar S, Rahamatolla M, Islam S, Jalil MA, Hossain S, Saeed MA, Bhuiyan MMR, Kazi F, Shekh S. Design, synthesis, and characterization of a novel pH-responsive azo dye incorporating a 1, 3, 4-thiadiazole ring for advanced textile applications. Dyes and Pigments. 2024; 231: 112410.*

32. ^*Kheirkhahi M, Shaabani B, Samadi Kafil H. Calix [4] arene-based thiosemicarbazide Schiff-base ligand and its transition metal complexes: synthesis and biological assessment. Journal of the Iranian Chemical Society. 2021; 18(12): 3429-3441.*

33. ^*Emam SM, Bondock S, Aldaloa AA. Schiff base coordination compounds including thiosemicarbazide derivative and 4-benzoyl-1, 3-diphenyl-5-pyrazolone: Synthesis, structural spectral characterization and biological activity. Results in Chemistry. 2023; 5: 100725.*

34. ^*Nehar OK, Mahboub R, Louhibi S, Roisnel T, Aissaoui M. New thiosemicarbazone Schiff base ligands: Synthesis, characterization, catecholase study and hemolytic activity. Journal of Molecular Structure. 2020; 1204: 127566.*

35. ^*Berber N. Preparation and characterization of some Schiff base compounds. Adıyaman University Journal of Science. 2020; 10(1): 179-188.*

36. ^*Bonnel C, Legrand B, Bantignies J-L, Petitjean H, Martinez J, Masurier N, Maillard LT. FT-IR and NMR structural markers for thiazole-based γ-peptide foldamers. Organic & Biomolecular Chemistry. 2016; 14(37): 8664-8669.*